Lignin-containing photoactive resins for 3D printing by stereolithography

Jordan T. Sutton[1,2], Kalavathy Rajan[1,3], David P. Harper*[1], Stephen C. Chmely*[1]

1. Center for Renewable Carbon, The University of Tennessee Institute of Agriculture, Knoxville, Tennessee 37996, United States

2. Department of Materials Science and Engineering, The University of Tennessee Knoxville, Knoxville, Tennessee 37996, United States

3. Department of Biosystems Engineering and Soil Science, The University of Tennessee Institute of Agriculture, Knoxville, Tennessee 37996, United States

Corresponding authors' email: dharper4@utk.edu, schmely@utk.edu

Keywords: lignin, 3D printing, stereolithography, additive manufacturing, resin

Abstract

Generating compatible and competitive materials that are environmentally sustainable and economically viable is paramount for the success of additive manufacturing using renewable materials. We report the successful application of renewable, modified lignin-containing photopolymer resins in a commercial stereolithography system. Resins were fabricated within operable ranges for viscosity and cure properties, using up to 15% modified lignin by weight with the potential for higher amounts. A four-fold increase in ductility in cured parts with higher lignin concentration is noted as compared to commercial SLA resins. Excellent print quality was seen in modified lignin resins, with good layer fusion, high surface definition, and visual clarity. These materials can be used to generate new products for additive manufacturing applications and help fill vacant material property spaces, where ductility, sustainability, and application costs are critical.

1. Introduction

Additive manufacturing offers greater freedom of design, quicker product development, and at a cheaper cost over traditional manufacturing techniques. In 2018, the global additive manufacturing (AM) market has a predicted value of $12.8 billion.[1] The complexity offered by greater design freedom means that parts can be topologically optimized to improve mechanical properties and hybrid materials can be designed that can achieve material properties unobtainable with conventional material processing.[2-3] However, one major hurdle for all AM technologies is in the design of new materials that are compatible with these AM processes but still comparable in cost and properties to those of traditional manufacturing. Renewable-sourced biomaterials are sustainable and abundant, giving them a competitive advantage over materials derived from fossil fuels. Hence, engineering novel biomaterials provides the opportunity to create cost-effective materials that reduce the environmental impact of additive manufacturing while meeting traditional material requirements.

Stereolithography (SLA) is an AM process that uses a bath of liquid photopolymer resin, a movable platform, and a laser UV source to cure resin layer by layer to build part geometries. The main limitation of SLA technology is the photopolymer build material. In the next decade, the market for 3D printing materials is expected to grow to at least $16 billion, and a significant portion of that is predicted to be shared by photopolymers.[1] Currently, these materials are few, limited in features, and expensive.[4]

Resins designed for AM processes are complex mixtures generally composed of a photoinitiator, monomers and oligomers, and other additives incorporated to achieve

53 specific properties. Photosensitizers and UV blockers, for instance, can be added to
54 shift cure wavelength and affect reaction kinetics.[5] Resin formulations are finely tuned to
55 work efficiently with the printer configuration and achieve the desired material
56 properties. As expected, these complex formulations are costly to design and produce.
57 In addition to cost, photopolymers typically exhibit issues with shrinkage, brittleness,
58 and slow cure speed. In SLA, these problems are related to the photopolymerization
59 reaction. Therefore, one approach to solving these problems is to control the reaction by
60 altering the resin formulation.

61 Lignin is the world's second-most abundant natural polymer, and the only high-
62 volume renewable feedstock composed of aromatics.[6] Most of the lignin available is
63 produced as a byproduct of cellulose production, and although much of it is used as a
64 fuel source for these processes, some methods can generate up to 60% more lignin
65 than is used during combustion.[7] In fact, by 2022, 62 million tons of lignin will be
66 produced annually.[8] Second-generation biofuels derived from lignocellulosic sources
67 are poised to play an important role in alternative energy solutions, and the economic
68 success of these biorefineries lies with co-product revenue streams.

69 Much work has gone toward the valorization of lignin for use in fuels, chemicals,
70 and polymers. For instance, lignin could be used to replace costly polyacrylonitrile as a
71 precursor material for producing carbon fibers (CF), and currently many groups are
72 working towards improving the performance of lignin-derived versus traditionally-made
73 CFs.[9-11] Lignin also shows great promise for use in other sustainable soft materials,[12]
74 and several commercially viable products containing lignin have been investigated.[13]

In contrast to simply blending technical lignin with existing petrochemical-based polymers, chemical modifications to isolated technical lignin typically lead to improved chemical, physical, and thermal properties of the resulting product. In fact, these can even offer additional functionality, such as an increase in photoactivity. For instance, bio-plastics developed from acylated model-lignin compounds like syringol, creosol, and vanillin were shown to possess enhanced thermal stability and tunable viscoelastic properties.[14-15] Bio-based epoxy resins made from depolymerized and glycidylated softwood lignin displayed superior flexural modulus and flexural strength.[16] Our group has also recently demonstrated that engineered hydrogels containing methacrylate-modified hardwood lignin exhibited increase in water retention capacity and tunable mechanical properties.[17] Moreover, alkene-functionalized lignin was successfully harnessed for photo-induced polymerization reactions.[18] In short, these studies demonstrate that designing lignin building blocks via chemical modification of the OH groups is a feasible approach for formulating 3D printing resins with tunable properties.

We are interested in developing transformations of lignin to make it amenable to incorporation into new high-performance engineered materials. Here, we report on our efforts to produce photoactive resins that contain organosolv lignin isolated from hybrid poplar. We formulated these resins by chemically modifying the lignin macromolecules to contain methacrylate moieties. Then, we blended the lignin with commercially available resin components to formulate a complete resin. We used a commercial desktop 3D printer from Formlabs to print with these resins, and report on the spectroscopic, mechanical, and thermal properties of these materials. This work

97 represents a platform from which the design of advanced photoactive resins for additive
98 manufacturing purposes can commence.

99

100 **2. Experimental Section**

101 **2.1. Reagents and materials.** Lignin was isolated from pulp-grade wood chips of
102 hybrid poplar (*Populus trichocarpa* × *P. deltoides*) using an ethanol organosolv
103 technique as described by Bozell and coworkers.[19] Ethoxylated pentaerthritol
104 tetraacrylate (SR494, Sartomer) and aliphatic urethane acrylate (Ebecryl 8210, Allnex)
105 were used as resin bases. A monofunctional urethane acrylate (Genomer 1122, Rahn)
106 was used as a reactive diluent. Diphenyl (2,4,6-trimethylbenzoyl) phosphine oxide (PL-
107 TPO, Esstech) and 2,2'-(2,5-thiophenediyl)bis(5-tert-butylbenzoxazole) (Benetex OB
108 Plus, Mayzo) were used as the resin photoinitiator and UV blocker, respectively.
109 Commercial PR48 resin was obtained from Colorado Photopolymer Solutions (Boulder,
110 CO) for comparison purposes. 2-chloro-4,4,5,5-tetramethyl-1,3,2-dioxaphospholane
111 (TMDP, Santa Cruz Biotechnology, Inc.) was stored in a vacuum desiccator to protect it
112 from atmospheric moisture. Endo-*N*-hydroxy-5-norbornene-2,3-dicarboximide (Sigma-
113 Aldrich) was used as received.

114 **2.2. Lignin modification for resin formulation.** The protocol for lignin acylation
115 (Scheme 1) was adapted from the method for syringyl methacrylate synthesis as
116 described by Epps and coworkers.[14-15] Methacrylic anhydride (Alfa Aesar) was allowed
117 to react with lignin (1.2 equiv of the lignin OH groups as measured by ^{31}P NMR) in the
118 presence of 4-dimethylaminopyridine (DMAP, Sigma-Aldrich) as a catalyst (0.04 equiv

of methacrylic anhydride). The reaction mixture was incubated at 60 °C for 48 hours and the lignin thus acylated (lignin-M) was purified by quenching the byproducts and unreacted substrate with a saturated solution of sodium bicarbonate. Lignin-M that precipitated during the reaction was washed with copious amounts of water until the washes reached neutral pH. The resulting precipitate was dried under reduced pressure at 40 °C for 48 hours and used for resin formulation.

Scheme 1. Synthesis scheme for lignin-M using methacrylic anhydride.

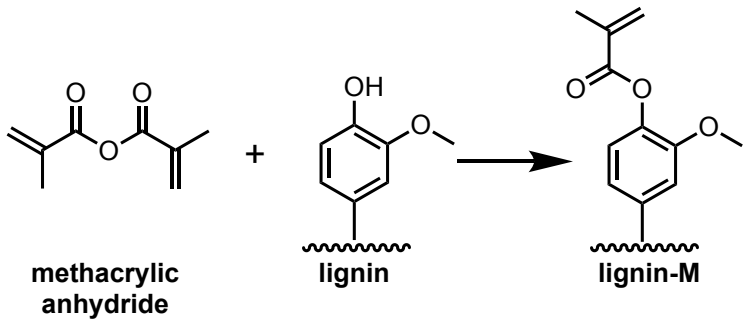

2.3. Lignin characterization. The hybrid poplar lignin and lignin-M were characterized using ^{31}P NMR and Fourier transform infrared (FTIR) spectroscopies to monitor the chemical changes in lignin and the efficiency of acylation reaction. Sample preparation and quantification of lignin OH groups was achieved using ^{31}P NMR spectroscopy as described by Balakshin and Capanema.[20] Briefly, the lignin samples were phosphitylated using TMDP, and the resulting NMR spectra were phased and referenced to the chemical shift of the water-derived complex of TMDP (δ 132.2 ppm). Quantification was achieved using endo-*N*-hydroxy-5-norbornene-2,3-dicarboximide as the internal standard. All ^{31}P NMR spectra were collected using a Varian 400-MR spectrometer (Varian Inc., Palo Alto, CA), operating at 161.92 MHz and 25 °C. FTIR spectra in the range of 4000 to 600 cm^{-1} were obtained using a UATR Spectrum Two

instrument (PerkinElmer, Llantrisant, UK), where the finely ground samples were analyzed at 16 scans per spectrum and 4 cm^{-1} resolution. The FTIR peaks were assigned based on previous reports,[21-23] and the spectra were subjected to statistical analysis using principal component analysis (PCA).

2.4. Resin formulation. The formulations of the 3-D printing resins used in this investigation are presented in Table 1. The photoinitiator and UV blocker were weighed and combined in a polypropylene container. The resin bases were added by weight in increasing viscosity as follows: the monofunctional urethane acrylate (Genomer 1122), the tetra-acrylate oligomer (SR494), and finally the aliphatic urethane acrylate (Ebecryl 8210). The partially formulated resin was mixed in a kinetic mixer (FlackTek, Speedmixer Dac 150 FVZ) at 2400 RPM for 0.5 min. Lignin-M was then weighed and added to the container and the resin was mixed again at 2400 RPM for 1 min. The lignin resins (LR) thus formulated (5-15% lignin by weight, LR5, LR10, and LR15) were stored in tightly sealed opaque containers to protect them from light.

Table 1. Composition of Modified Resins

Resin	SR494 (wt%)	Ebecryl 8210 (wt%)	Genomer 1122 (wt%)	Lignin-M (wt%)	PL-TPO (wt%)	Mayzo OB+ (wt%)
PR48	39.78	39.78	19.89	0	0.4	0.16
LR5	37.84	37.84	18.92	5	0.4	0
LR10	35.84	35.84	17.92	10	0.4	0
LR15	33.84	33.84	16.92	15	0.4	0

2.5. Resin working curves. All resins were characterized for critical cure dosage and penetration depth parameters using the working curve method outlined elsewhere.[24] This method relies on a relationship between cure thickness and dosage derived from the Beer-Lambert Law as shown below:

$$C_d = D_p \cdot \ln(E) - D_p \cdot \ln(E_{crit}) \quad (1)$$

where C_d is the cure depth, D_p is the penetration depth, E_{crit} is the critical dosage exposure required to cure the resin, and E is the dosage applied per layer. This dosage can be controlled by the laser scan velocity in accordance with the following relation:

$$E = \frac{P_L}{V_s h_s} \quad (2)$$

where V_s is the scan line velocity, h_s is the scan line spacing, and P_L is the laser power. Together, equations 1 and 2 can be used to experimentally determine D_p and E_{crit}, since a plot of cure depth (thickness) versus the natural log of dosage (E) can be fit with a line whose slope is penetration depth (D_p) and whose y-intercept (b) is given as

$$b = -D_p \cdot \ln(E_{crit}) \quad (3)$$

A rectangular model was designed using AutoCAD (Autodesk, Inc., San Rafael, CA) having dimensions 40 × 64 mm^2. It was composed of 32 squares that had varying thickness ranging from 5 to 20 layers. The model was printed directly on the resin bath to ensure that the resultant thicknesses were due only to the applied dosage. The 3D printed specimen was removed from the bath and cleaned of excess resin. The material thickness was measured for each square using a digital Vernier caliper and plotted against the natural log of the dosage. A linear regression was performed on the data to

175 obtain the slope (corresponding to D_p) and y-intercept (related to the critical dosage as
176 described by equation 3 above).

177 **2.6. 3D printing using lignin resins by stereolithography.** Models for 3D
178 printing were designed in AutoCAD, and all samples were generated using a Formlabs
179 (Formlabs, Inc., Somerville, MA) Form 1+ desktop stereolithography (SLA) printer,
180 installed with a modified version of the printer's software called OpenFL. The SLA
181 printer used a 120 mW Class-1 laser emitting at 405 nm, and had a build volume of 125
182 × 125 × 165 mm^3. The 3D printing resins were stored and used at room temperature.
183 Custom print files for each resin were designed using dose calculations obtained from
184 the resin working curves. The laser settings for printing the LR resins were obtained by
185 modifying the laser-scan velocity that delivered the necessary dosage, as per eqn. (2).
186 Print files were designed to cure the resins of 50 μm thickness. OpenFL was used to
187 generate the scaffolds before printing. Tensile bars were built at a 45° angle with
188 scaffolds edited to avoid placement along the gauge length.

189 The printed parts were separated from the build platform and soaked in two
190 consecutive baths of isopropanol for 10 min each to remove any uncured resin and
191 scaffolds. A 400 W metal halide UV (arc) lamp (Uvitron International Inc., West
192 Springfield, MA), with irradiance capacity of 200 mW/cm^2 at a height of 7.62 cm was
193 used to post-cure the printed parts for 3 min.

194 **2.7. Materials characterization.** The viscosity of the formulated resins was
195 measured using a TA Instruments AR-G2 rheometer with cone and plate geometry. The
196 rheometer was configured with a 40 mm diameter cone at a truncation gap of 56 μm.
197 Tests were performed over a range of shear rates from 0.1 to 100 Hz at 25 °C.

198 Chemical characterization of the cured samples was performed using FTIR
199 spectroscopy, where the solids samples were directly analyzed on the crystal of an ATR
200 accessory attachment. Five individual spectra were collected for all samples.
201 Thermogravimetric analysis (TGA) was performed using a PerkinElmer Pyris 1 TGA.
202 Each test was programmed to run from 30 °C to 900 °C at a heating rate of 20 °C/min.
203 All tests were done under a continuous nitrogen flow of 10 mL/min.

204 Ultimate tensile strength and Young's modulus of the cured samples were
205 obtained using an Instron 5567 dual column universal testing machine. A 30 kN static
206 load cell was used. Tests were performed following the ASTM D638 standard according
207 to type V specimen dimensions. A 1 mm/min extension rate was applied for all tests.
208 Scaffold marks on printed samples were removed by sanding prior to testing to avoid
209 any stress concentration.

210 Scanning electron microscopy (SEM) was performed using a Phenom ProX with
211 an accelerating voltage of 10 kV. Samples were cut to size and cleaned of debris prior
212 to mounting.

213 **3. Results and Discussion**

214 **3.1. Modified lignin characterization.** Lignin-M, obtained via acylation of OH
215 groups of hybrid poplar lignin with methacrylic anhydride (Scheme 1), was characterized
216 using ^{31}P NMR and FTIR spectroscopy. Figure 1a depicts the FTIR spectra, in which
217 lignin-M had a significant reduction in OH functional groups (3403 cm^{-1}). This is
218 expected, as the number of OH groups is depleted as the acylation reaction takes place
219 (Scheme 1). The FTIR spectra indicate an increase in methacrylate functional groups

attached to the modified lignin OH groups, as evidenced by increases in peaks corresponding to C=O stretches, C-O-C stretches, and in plane $–CH_2$ bending vibrations (1723, 1131 and 943 cm^{-1}, respectively).

^{31}P NMR spectroscopy is another method used to quantify the changes in lignin OH groups, and is particularly useful to detect differences among substitution at the aliphatic, syringyl (S), guaiacyl (G), para-hydroxy (H), and carboxylic acid (COOH) hydroxyl groups. As shown in Figure 1b, OH groups in lignin-M undergo substantial substitution, where 92% of these are acylated. The scant amounts of COOH groups (0.1 mmol/g) observed in lignin-M might have originated from residual methacrylic acid, which is a byproduct of lignin modification.

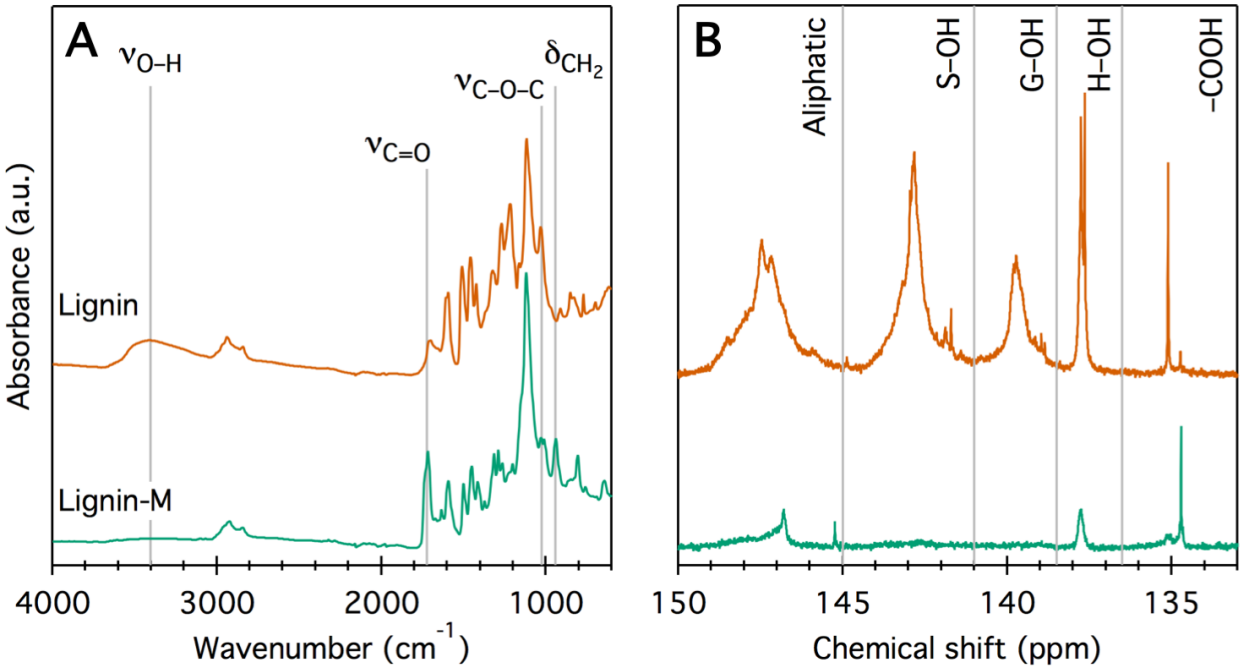

Figure 1. (A) Fourier transform infrared spectra of hybrid poplar lignin before (top, brown) and after (bottom, green) methacrylate modification of the OH groups to afford lignin-M. Disappearance of the ν_{O-H} peak indicates substitution at the hydroxyl groups,

234 and an increase in $\nu_{C=O}$, ν_{C-O-C}, and δ_{CH2} indicate the presence of a methacrylate
235 moiety. (B) ^{31}P NMR spectra of the same samples (color scheme and position identical)
236 with integration ranges (taken from Balakshin and Capanema[20]) also indicate
237 substitution at the hydroxyl groups, including the syringyl, guaiacyl, and p-hydroxy (S,
238 G, and H, respectively) aromatic hydroxyl groups. The shifted –COOH peak in lignin-M
239 is due to residual methacrylic acid, a byproduct of the methacrylation reaction.

240 **3.2. LR formulations.** We used lignin-M as a source of acrylate oligomers and
241 reactive diluent at 5 to 15% by weight to formulate our 3D printing resins. To ensure that
242 lignin-M was incorporated into the resin bases homogenously, we created the LR
243 mixtures in small batches and allowed them to rest for 48 h. Unmodified lignin dissolved
244 poorly in acrylate-based resins, whereas lignin-M showed significant improvement in
245 homogeneity owing to the compatibility of its methacrylate functional groups (Figure
246 S1).

247 We identified resin viscosity as a critical parameter for compatibility with an
248 additive printing mechanism because of its role in affecting the resin recoating
249 procedure over the curing surfaces between two contiguous layers. Fast laser scan
250 speeds meant that, in general, the speed at which the part can be printed is determined
251 by how quickly the printer can reset for a new layer. Higher viscosities result in longer
252 wait times for the recoating procedure and overall longer printing duration. The viscosity
253 measurements for LR5-15 (Figure 2) showed that they displayed Newtonian behavior
254 and had a viscosity range from 0.44 to 1.66 Pa·s. Commercial manufacturers have
255 reported viscosities in the ranges of 0.85 to 4.5 Pa·s for their 3D printing resins, so LR5-
256 15 are evidently viable for creating equivalent print designs. The measured viscosity of

257 LR5-15 increased with increasing lignin-M content, which implies a limit to the amount
258 of lignin the base resin can host and still be within a usable viscosity range without
259 additional diluent.

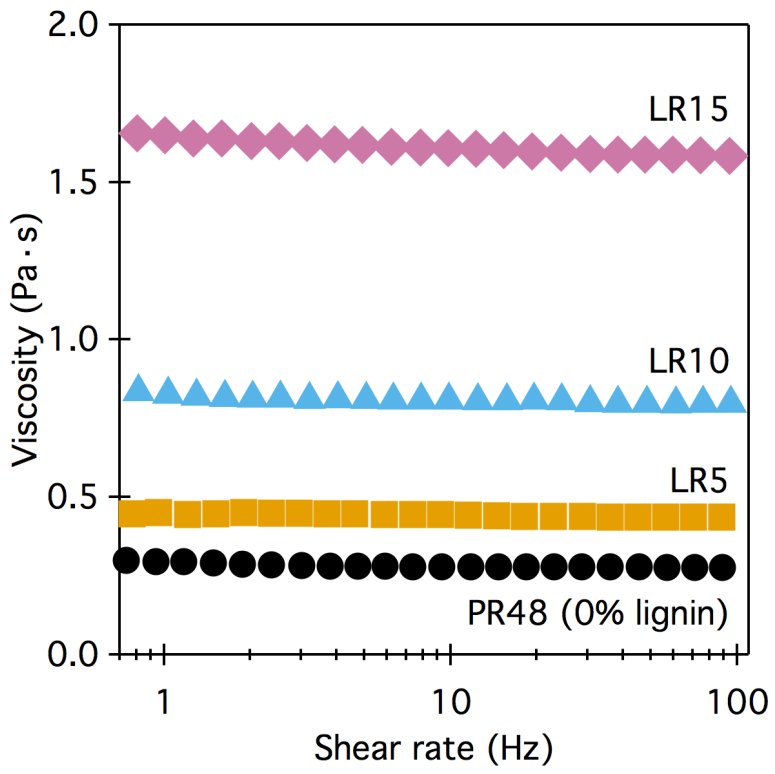

260

261 **Figure 2.** Plot of viscosity versus shear rate of photo curable acrylate resins containing
262 various amounts of lignin-M. Viscosity increases with increasing amounts of lignin as
263 compared to the commercial PR48 resin.

264 **3.3. Resin cure properties**. The working curve approach is a basic model for
265 formulating SLA resins, since it provides a measurement of threshold energy required to
266 initiate photopolymerization (E_{crit}) and also helps to evaluate the resin cure properties.[24]
267 The working curves generated for all LR formulations are shown in Figure 3, and the
268 corresponding cure properties are listed in Table 2, along with the target dosage for a

printing a layer with a thickness of 50 μm (a photograph of the windowpane rectangle used to generate working curves is provided as Figure S2).

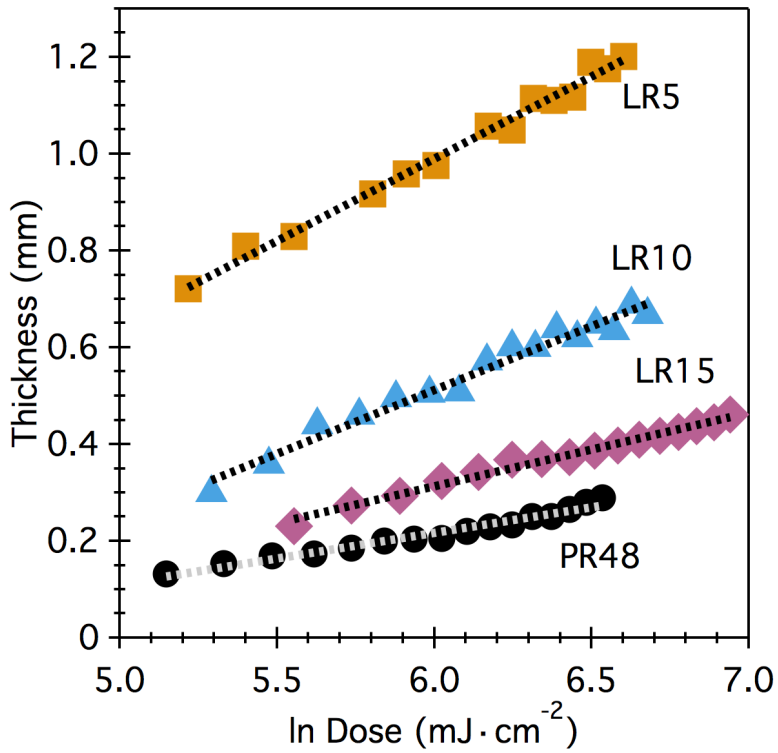

Figure 3. Working curves showing cure thickness as a function of the natural log of UV dosage for PR48 and LR formulations. Linear regressions are shown as dotted lines, and the related values are tabulated in Table 2 from Equations 1-3 above.

Penetration depth (D_p) is the distance photons travel in the resin before they are absorbed by a resin component. Resins with high D_p will allow more photons to pass farther into the resin, causing it to potentially cure thicker than a resin with a lower D_p. This results in poor resolution control and nonuniformity in the build geometry. Typically, SLA resins contain a UV blocker (Mayzo OB+ in PR48, see Table 1) to tune the D_p and reduce the required precision during printing.

Since lignin contains several UV-active moieties (aromatic rings and C=O bonds), we expected that it would readily absorb UV photons and potentially serve the same role as the UV blocker. Consequently, we prepared all LR formulations without Mayzo OB+. As is evident from the data in Table 2, even up to 15 wt-% lignin-M, Dp for the LR formulations was still higher than that for PR48, which contains 0.16 wt-% UV blocker. Surprisingly, the added lignin does not appear to retard the penetration of the UV photons required to initiate the polymerization reactions. As expected, D_p decreased in resins with higher amounts of incorporated lignin-M. The photoactivity of lignin results in light scattering and absorption, which reduces the transmission through the resin. Evidently, lignin-M in the LR resins could act not only as a structural feature but also as a UV blocker, owing to its ability to scatter and absorb photons. We are currently investigating the efficacy of lignin to be used as a specialized UV blocker in these formulations.

Table 2. Cure parameters for tested resin formulations

Resin Formulation	D_p (mm)	E_{crit} ($J \cdot cm^{-2}$)
PR48	0.105(5)	0.05(2)
LR5	0.34(1)	0.022(5)
LR10	0.26(1)	0.06(2)
LR15	0.152(5)	0.05(1)

Relative uncertainties in the final digit are reported in parentheses.
D_p: penetration depth; E_{crit}: Critical cure dosage

298 Interestingly, the critical cure dosage (E_{crit}) was lower for the lignin-M containing
299 resins, even at 15-wt% loading. Although a higher critical cure dosage will result in a
300 larger starting dosage and could significantly increase the curing time, evidently the
301 presence of lignin does not deter resin curing. However, since the LR formulations do
302 not include a UV blocker, the presence of which would increase the critical cure dosage,
303 we are unable to unambiguously determine the reason for the change in E_{crit}. There is
304 certainly a complex interplay between penetration depth and critical cure dosage that
305 depends upon the amount of lignin in each sample, since lignin is known to be excited
306 by UV light and quench the free radicals by undergoing redox reactions resulting in the
307 formation of quinones.[25] We are currently investigating these phenomena further.

308 **3.4. Characterization of 3D printed and cured resins.** We used FTIR
309 spectroscopy of the polymerized resins and analysis of FTIR spectra (Figure S3) by
310 PCA to probe the chemical structure of the cured resins. From these, we determined
311 that the lignin-M containing polymers were significantly different than the control (Figure
312 4a).

313 As indicated by the PC1 loadings plot (Figure 4b), the largest difference between
314 PR48 and the LR formulations is due to the presence of unconjugated carbonyl bonds
315 (C=O), acrylate ester bonds (C-O-C) and in-plane bending of C=C groups (1723, 1191,
316 and 1407 cm^{-1}, respectively) in PR48. These can be attributed to unreacted acrylate
317 groups in PR48 due to an incomplete cure. We further observed these results from
318 scanning electron micrographs (vide infra) which we attribute to sub-optimal printing
319 parameters (see Figure 6 below). This suggests that the LR formulations were more
320 fully cured than the commercial PR48 formulation using the printing parameters we

selected. Additionally, the PC2 loadings plot (Figure 4c) indicates that LR15 displayed higher asymmetric and symmetric stretching vibrations of C–H bonds (at 2923 and 2855 cm^{-1}, respectively). This could possibly be attributed to the additional aliphatic groups in lignin, although this difference between the resins is relatively minor as reflected by the low percentage of contribution to the data variance (15%).

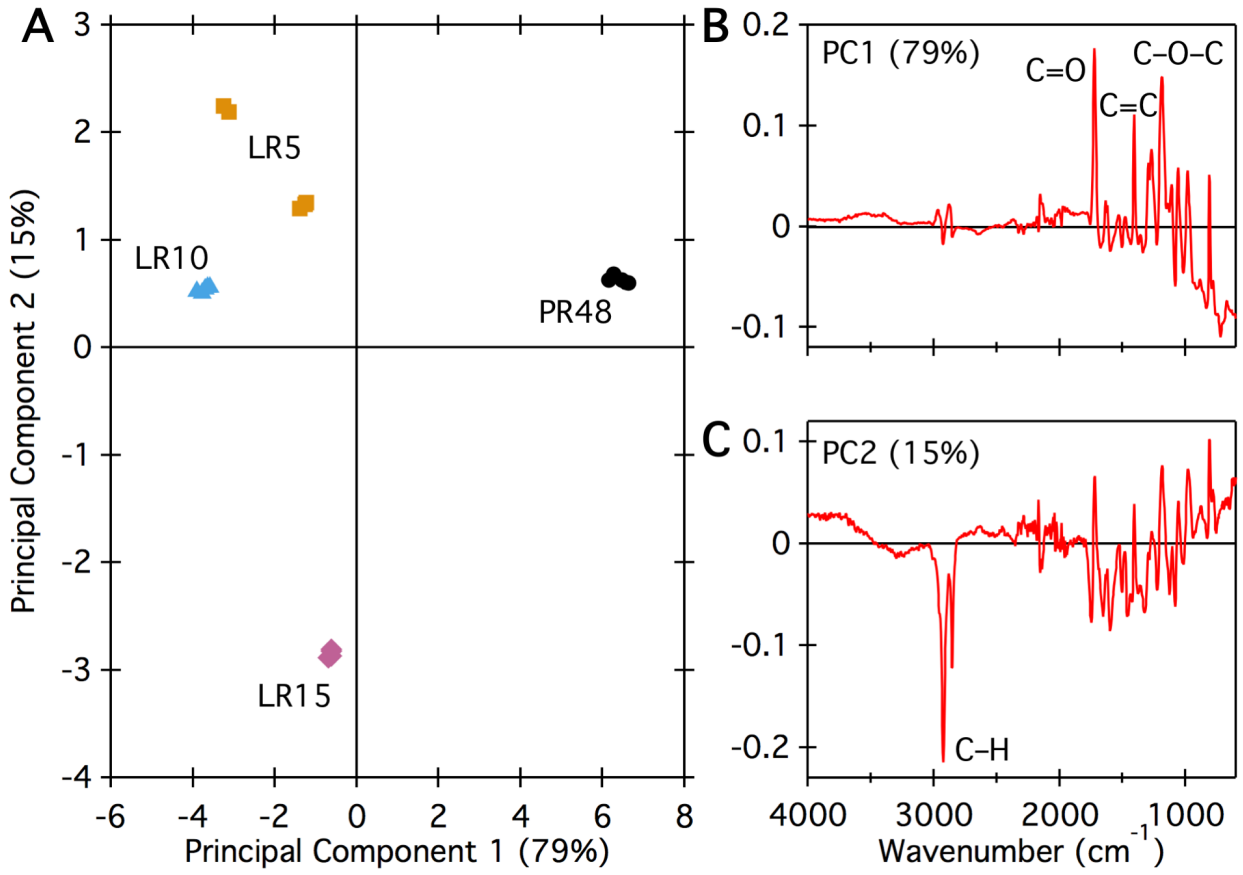

Figure 4. (A) Scores plot of the principal component analysis (PCA) of the FTIR spectra of printed and cured PR48, LR5, LR10, and LR15 resin formulations. The labeling scheme is identical to Figure 2. (B) Loadings plot of principal component 1 (PC1), which accounts for 79% of the data variance. Stretching frequencies for C=O, C=C, and C–O–

C moieties are noted. (C) Loadings plot of PC2, which accounts for 15% of the data variance. Stretching frequencies for C–H moieties are noted.

We performed tensile tests on the cured resins, and the results of these experiments are summarized in Table 3. Interestingly, the cured resins displayed a transition from brittle to ductile behavior in those that contain lignin-M. The elastic modulus showed a 43% decrease from 0.65 GPa with no lignin to 0.37 GPa with 15% lignin-M. Likewise, the ductility increased from a measured 1.87% elongation at break for the control to 7.62% for LR15. This indicated that lignin-M was acting as a plasticizer in the resin system. We attribute this phenomenon to the fact that the modified lignin molecules were introducing side chains in the polyacrylate that reduced the chain-to-chain interaction forces.[26] Photopolymers are usually brittle, so such an improvement could prove useful in increasing the toughness of parts printed by stereolithography.

Table 3. Mechanical testing of molded resins

Resin	**E (GPa)**	**σ_R (MPa)**	**ε_R (%)**
PR48	0.65(5)	11.0(4)	1.87(8)
LR5	0.64(2)	11(1)	3.0(1)
LR10	0.48(2)	18(3)	6(1)
LR15	0.37(2)	15(8)	7.6(1)

Relative uncertainties in the final digit are reported in parentheses.
E: tensile modulus; σ_R: failure stress; ε_R: strain at break

We used thermogravimetric analysis (TGA) of the printed and cured resins to study the thermal properties of these materials. TGA data (Figure 5) demonstrate that the cured LR resins exhibited different degradation onset temperatures when compared

349 to the control. The mechanism of thermal decomposition of cured polyacrylate resins
350 such as PR48 and the related LR formulations has been the focus of intense
351 investigation by several groups. The rate of thermal decomposition of PR48 accelerates
352 as the temperature increases as evident by the first derivative of the TG curve (Figure 5,
353 inset). This phenomenon is known to be due to a complex combination of kinetically
354 regulated chain scission and depolymerization reactions.[27] In case of the cured LR
355 formulations, we attribute the small weight loss at about 185 °C to scission of the ether
356 bonds that link lignin-M to the growing polyacrylate polymer and the related
357 decomposition of the lignin-M oligomers, owing to the enhanced lability of C–O bonds in
358 comparison to C–C bonds.[28]

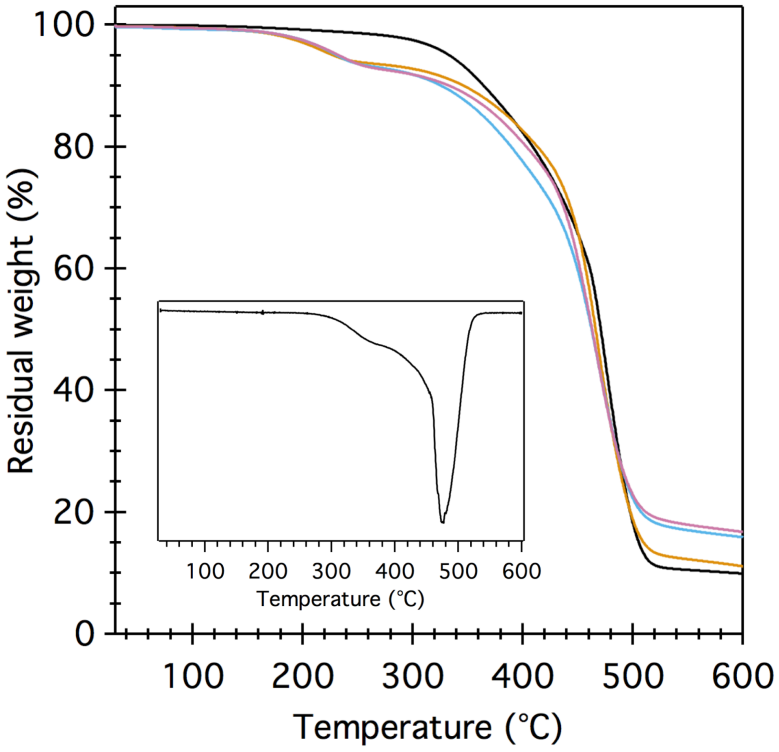

359

360 **Figure 5.** TGA curves (color scheme identical to Figure 2) for 3D printed commercial
361 PR48 resin and LR formulations. The derivative of the weight curve (inset)

362 demonstrates the change in rate of thermal decomposition of PR48. The decomposition
363 of the LR formulations at ~185 °C is evidence of thermolysis of the ether bonds that link
364 lignin-M to the poly(acrylate) backbone.

365 **3.5. Morphology and print quality.** We used scanning electron microscopy to
366 characterize the 3D printed surfaces (Figure 6). The surface of cured PR48 showed
367 significant gaps between layers, due to a lack of fusion between them. These defects
368 were regularly aligned along the edges of the line scan width where the dosage will be
369 at minimum, whereas the fusion at the center of the cross-line scans extended between
370 the layers. Since the print did not fail on the build platform, we attribute this
371 phenomenon to a higher required UV dosage to attain inter-layer adhesion in PR48.
372 Evidently, at the print settings we have chosen for this study, optimal addition of lignin-M
373 could enhance the photo-reactivity of the acrylate resins, thereby producing better prints
374 at lower UV dosages.

375 LR5 provided the best print quality with relatively smooth surfaces and excellent
376 layer adhesion, despite printing with the fastest laser scan velocity and at the lowest
377 dosage. Print surfaces for LR10 and LR15 had small regions of poor fusion along print
378 lines. These voids tended to be grouped together, suggesting that the presence of
379 lignin-M disrupted the assemblage of polyacrylates due to cross-linking with lignin.
380 Excepting these small regions, the surfaces of the 3D printed LR formulations showed
381 complete fusion between layers, which emphasizes not only that lignin-M is compatible
382 with SLA technology at the print layer level, but also that lignin-M shows great potential
383 as a binding agent for improved print quality.

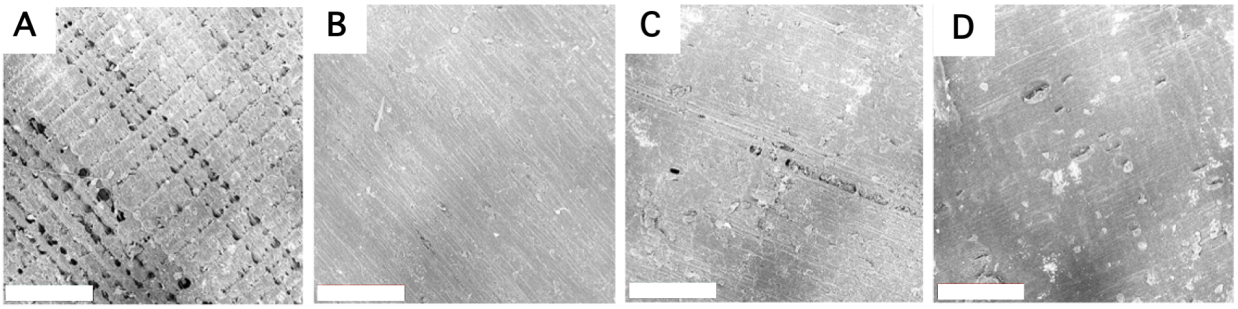

Figure 6. SEM images of the print surfaces for PR48 (A), LR5 (B), LR10 (C), and LR15 (D) showing an increase in surface roughness for LR formulations. Scale bars (white rectangles) denote 300 μm.

Visual evaluation of the print quality showed that the LR formulations displayed good build geometries compared to that of the commercial resin (Figure 7). High resolution and edge definition is achieved with the designed print settings. A significant degree of curling is present in the cured LR5 print because of the fast cure rate. Faster cure rates generally result in uneven shrinkage, causing a build-up of residual stresses and deformation of the material. Shrinkage can be reduced in this case either by modifying the resin formulation such that it has better cure properties or by changing the post-cure process. We did not observe this problem in the slower curing LR10 print. Transparency was reduced with higher amounts of lignin-M, but the resins did not cure fully opaque. Thus, pigmentation could be applied to change the resin color, however, the brown coloration of lignin may limit the range of colors that could be used successfully.

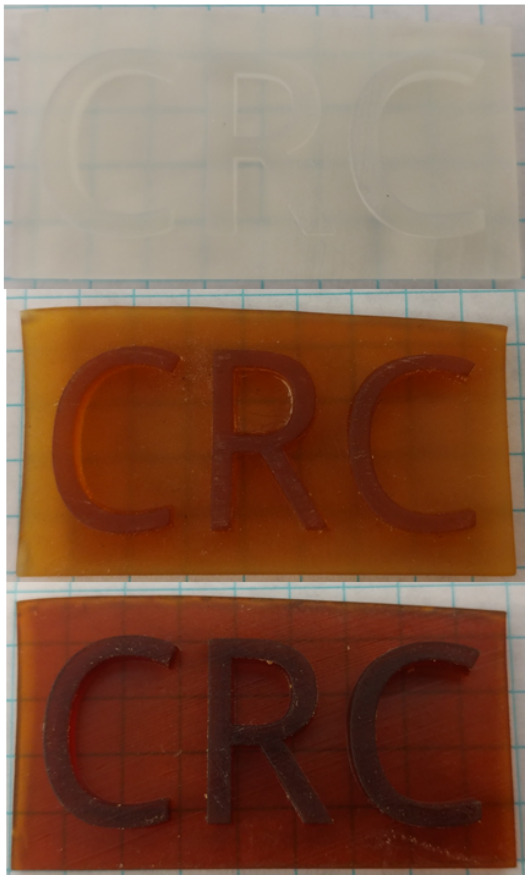

Figure 7. Photographs of 0% (PR48, top), 5% (LR5, middle), and 10% (LR10, bottom) lignin showing the effect on print quality. Even lignin-containing samples show translucence, suggesting they are amenable to pigmentation.

4. Conclusions

In this work, we generated new photo-active acrylate resins by mixing commercially available resin components with acylated organosolv lignin. The resulting mixtures contained up to 15% by weight lignin and were used to produce 3D prints via SLA technology. The lignin-containing resin formulations exhibited increased ductility but decreased thermal stability when compared to the commercially available control resin. Overall, we used the LR formulations to generate uniformly fused, high-resolution

prints that display enhanced material toughness with a lower UV dosage. Future work will focus on investigating the role that lignin plays as a UV blocker in these resin formulations and using strategies to link functional monomers to lignin using C–C bonds instead of thermally labile C–O bonds.

Acknowledgments

This project was supported by funds from the University of Tennessee AgResearch Innovation Fund. Additional funds were provided by the Southeastern Sun Grant Center and the US Department of Transportation, Research and Innovative Technology Administration DTOS59-07-G-00050. D.P.H. and S.C.C. also acknowledge support from the USDA National Institute of Food and Agriculture, Hatch Project 1012359.

References

1. Wohlers, T. T.; Caffrey, T., *Wohlers report 2015 : 3D printing and additive manufacturing state of the industry annual worldwide progress report*. Wohlers Associates: Fort Collins, Colo., 2015; p 314 p.

2. Ashby, M., Hybrid Materials to Expand the Boundaries of Material-Property Space. *J Am Ceram Soc* **2011,** *94*, S3-S14. DOI: 10.1111/j.1551-2916.2011.04559.x

3. Babu, S. S.; Goodridge, R., Additive manufacturing. *Mater Sci Tech-Lond* **2015,** *31* (8), 881-883. DOI: 10.1179/0267083615z.000000000929

4. Melchels, F. P. W.; Feijen, J.; Grijpma, D. W., A review on stereolithography and its applications in biomedical engineering. *Biomaterials* **2010,** *31* (24), 6121-6130. DOI: 10.1016/j.biomaterials.2010.04.050

5. Gibson, I.; Rosen, D.; Stucker, B., Vat Photopolymerization Processes. In *Additive Manufacturing Technologies : 3D Printing, Rapid Prototyping, and Direct Digital Manufacturing*. 2nd ed.; Springer: New York, NY, 2015; pp 63-106.

6. Tuck, C. O.; Perez, E.; Horvath, I. T.; Sheldon, R. A.; Poliakoff, M., Valorization of Biomass: Deriving More Value from Waste. *Science* **2012,** *337* (6095), 695-699. DOI: 10.1126/science.1218930

7. Sannigrahi, P.; Ragauskas, A. J., Characterization of Fermentation Residues from the Production of Bio-Ethanol from Lignocellulosic Feedstocks. *J Biobased Mater Bio* **2011,** *5* (4), 514-519. DOI: 10.1166/jbmb.2011.1170

8. Ragauskas, A. J.; Beckham, G. T.; Biddy, M. J.; Chandra, R.; Chen, F.; Davis, M. F.; Davison, B. H.; Dixon, R. A.; Gilna, P.; Keller, M.; Langan, P.; Naskar, A. K.; Saddler, J. N.; Tschaplinski, T. J.; Tuskan, G. A.; Wyman, C. E., Lignin Valorization: Improving Lignin Processing in the Biorefinery. *Science* **2014,** *344* (6185), 709-+. DOI: ARTN 124684310.1126/science.1246843

9. Hosseinaei, O.; Harper, D. P.; Bozell, J. J.; Rials, T. G., Role of Physicochemical Structure of Organosolv Hardwood and Herbaceous Lignins on Carbon Fiber Performance. *ACS Sustainable Chemistry & Engineering* **2016,** *4* (10), 5785-5798. DOI: 10.1021/acssuschemeng.6b01828

10. Hosseinaei, O.; Harper, D. P.; Bozell, J. J.; Rials, T. G., Improving Processing and Performance of Pure Lignin Carbon Fibers through Hardwood and Herbaceous Lignin Blends. *International Journal of Molecular Sciences* **2017,** *18* (7). DOI: 10.3390/ijms18071410

11. Mainka, H.; Tager, O.; Korner, E.; Hilfert, L.; Busse, S.; Edelmann, F. T.; Herrmann, A. S., Lignin - an alternative precursor for sustainable and cost-effective automotive carbon fiber. *J Mater Res Technol* **2015,** *4* (3), 283-296. DOI: 10.1016/j.jmrt.2015.03.004

12. Upton, B. M.; Kasko, A. M., Strategies for the Conversion of Lignin to High-Value Polymeric Materials: Review and Perspective. *Chem Rev* **2016,** *116* (4), 2275-2306. DOI: 10.1021/acs.chemrev.5b00345

13. Graichen, F. H. M.; Grigsby, W. J.; Hill, S. J.; Raymond, L. G.; Sanglard, M.; Smith, D. A.; Thorlby, G. J.; Torr, K. M.; Warnes, J. M., Yes, we can make money out of lignin and other bio-based resources. *Industrial Crops and Products* **2017,** *106*, 74-85. DOI: 10.1016/j.indcrop.2016.10.036

14. Holmberg, A. L.; Nguyen, N. A.; Karavolias, M. G.; Reno, K. H.; Wool, R. P.; Epps, T. H., Softwood Lignin-Based Methacrylate Polymers with Tunable Thermal and Viscoelastic Properties. *Macromolecules* **2016,** *49* (4), 1286-1295. DOI: 10.1021/acs.macromol.5b02316

15. Holmberg, A. L.; Reno, K. H.; Nguyen, N. A.; Wool, R. P.; Epps, T. H., Syringyl Methacrylate, a Hardwood Lignin-Based Monomer for High-T-g Polymeric Materials. *Acs Macro Lett* **2016,** *5* (5), 574-578. DOI: 10.1021/acsmacrolett.6b00270

16. van de Pas, D. J.; Torr, K. M., Biobased Epoxy Resins from Deconstructed Native Softwood Lignin. *Biomacromolecules* **2017,** *18* (8), 2640-2648. DOI: 10.1021/acs.biomac.7b00767

17. Rajan, K.; Mann, J. K.; English, E.; Harper, D. P.; Carrier, D. J.; Rials, T. G.; Labbé, N.; Chmely, S. C., Sustainable Hydrogels Based on Lignin-Methacrylate Copolymers with Enhanced Water Retention and Tunable Material Properties. *Biomacromolecules* **2018,** *19* (7), 2665-2672. DOI: 10.1021/acs.biomac.8b00282

18. Liu, H.; Chung, H., Visible-Light Induced Thiol–Ene Reaction on Natural Lignin. *ACS Sustainable Chemistry & Engineering* **2017,** *5* (10), 9160-9168. DOI: 10.1021/acssuschemeng.7b02065

19. Bozell, J. J.; Black, S. K.; Myers, M.; Cahill, D.; Miller, W. P.; Park, S., Solvent fractionation of renewable woody feedstocks: Organosolv generation of biorefinery process streams for the production of biobased chemicals. *Biomass Bioenerg* **2011,** *35* (10), 4197-4208. DOI: 10.1016/j.biombioe.2011.07.006

20. Balakshin, M.; Capanema, E., On the Quantification of Lignin Hydroxyl Groups with P-31 and C-13 Nmr Spectroscopy. *J Wood Chem Technol* **2015,** *35* (3), 220-237. DOI: 10.1080/02773813.2014.928328

21. Schwanninger, M.; Rodrigues, J. C.; Pereira, H.; Hinterstoisser, B., Effects of short-time vibratory ball milling on the shape of FT-IR spectra of wood and cellulose. *Vib Spectrosc* **2004,** *36* (1), 23-40. DOI: 10.1016/j.vibspec.2004.02.003

22. Lv, P.; Almeida, G.; Perré, P., TGA-FTIR Analysis of Torrefaction of Lignocellulosic Components (cellulose, xylan, lignin) in Isothermal Conditions over a Wide Range of Time Durations. *Bioresources* **2015,** *10* (3). DOI: 10.15376/biores.10.3.4239-4251

23. Udagawa, A.; Sakurai, F.; Takahashi, T., In situ study of photopolymerization by fourier transform infrared spectroscopy. *Journal of Applied Polymer Science* **1991,** *42* (7), 1861-1867. DOI: 10.1002/app.1991.070420707

24. Jacobs, P. F.; Reid, D. T., *Rapid prototyping & manufacturing : fundamentals of stereolithography*. 1st ed.; Society of Manufacturing Engineers in cooperation with the Computer and Automated Systems Association of SME: Dearborn, MI, 1992; p 434 p.

25. Castellan, A.; Grelier, S.; Kessab, L.; Nourmamode, A.; Hannachi, Y., Photophysics and photochemistry of a lignin model molecule containing α-carbonyl guaiacyl and 4-hydroxy-3-methoxybenzyl alcohol moieties. *J. Chem. Soc., Perkin Trans. 2* **1996,** (6), 1131-1138. DOI: 10.1039/p29960001131

26. Immergut, E. H.; Mark, H. F., Principles of Plasticization. In *Plasticizationand Plasticizer Processes*; Platzer, N. A. J., Eds.; American Chemical Society: Washington, DC, 1965; pp 1-26. DOI: 10.1021/ba-1965-0048.ch001

27. Holland, B. J.; Hay, J. N., The kinetics and mechanisms of the thermal degradation of poly(methyl methacrylate) studied by thermal analysis-Fourier transform infrared spectroscopy. *Polymer* **2001,** *42* (11), 4825-4835. DOI: 10.1016/s0032-3861(00)00923-x

28. Kim, S.; Chmely, S. C.; Nimlos, M. R.; Bomble, Y. J.; Foust, T. D.; Paton, R. S.; Beckham, G. T., Computational Study of Bond Dissociation Enthalpies for a Large Range of Native and Modified Lignins. *The Journal of Physical Chemistry Letters* **2011,** *2* (22), 2846-2852. DOI: 10.1021/jz201182w